

Nature of Partial Magnetic Order in the Frustrated Antiferromagnet $\text{Gd}_2\text{Ti}_2\text{O}_7$

Joseph A. M. Paddison,^{1,2,3,4,*} Georg Ehlers,⁵ Andrew B. Cairns,³ Jason S. Gardner,⁶ Oleg A. Petrenko,⁷ Nicholas P. Butch,⁸ Dmitry D. Khalyavin,⁴ Pascal Manuel,⁴ Henry E. Fischer,⁹ Haidong Zhou,^{10,11} Andrew L. Goodwin,³ and J. Ross Stewart^{4,†}

¹Materials Science and Technology Division, Oak Ridge National Laboratory, Oak Ridge, TN 37831, USA

²Churchill College, University of Cambridge, Storey's Way, Cambridge CB3 0DS, U.K.

³Department of Chemistry, University of Oxford, Inorganic Chemistry Laboratory, South Parks Road, Oxford OX1 3QR, U.K.

⁴ISIS Neutron and Muon Source, Rutherford Appleton Laboratory, Didcot OX11 0QX, U.K.

⁵Neutron Technologies Division, Oak Ridge National Laboratory, Oak Ridge, TN 37831, USA

⁶Songshan Lake Materials Laboratory, Dongguan, Guangdong 523808, China

⁷Department of Physics, University of Warwick, Coventry CV4 7AL, U.K.

⁸NIST Center for Neutron Research, National Institute of Standards and Technology, Gaithersburg, MD 20899, USA

⁹Institut Laue-Langevin, 71 Avenue des Martyrs, CS 20156, 38042 Grenoble Cedex 9, France

¹⁰Department of Physics and Astronomy, University of Tennessee, Knoxville, TN 37996, USA

¹¹National High Magnetic Field Laboratory, Florida State University, Tallahassee, FL 32310, USA

(Dated: November 16, 2021)

Partially-ordered magnets are distinct from both spin liquids and conventional ordered magnets because order and disorder coexist in the same magnetic phase. Here, we determine the nature of partial order in the canonical frustrated pyrochlore antiferromagnet $\text{Gd}_2\text{Ti}_2\text{O}_7$. Using single-crystal neutron-diffraction measurements in applied magnetic field, magnetic symmetry analysis, inelastic neutron-scattering measurements, and spin-wave modeling, we show that its low-temperature magnetic structure involves two propagation vectors (2- \mathbf{k} structure) with suppressed ordered magnetic moments and enhanced spin-wave fluctuations. Our experimental results support theoretical predictions of thermal fluctuation-driven order in $\text{Gd}_2\text{Ti}_2\text{O}_7$.

Geometrical frustration is a central theme of condensed-matter physics because it can generate exotic magnetic states. These states can typically be divided into spin liquids, in which frustration inhibits long-range magnetic order, and spin solids, in which perturbations to the dominant frustrated interactions drive magnetic order [1]. Defying this classification, some frustrated magnets exhibit *partial* magnetic order [2–8]—the coexistence of order and disorder in the same magnetic phase. Magnetic partial order can be driven by fluctuations in an “order-by-disorder” scenario [9], by interactions between emergent degrees of freedom in spin-fragmented states [10–12], or by proximity to a quantum critical point [13], while structural partial order can drive the behavior of materials such as fast-ion conductors [14, 15], Pb-based photovoltaics [16, 17], and high-pressure elemental phases [18]. To benchmark theories of partially-ordered states [9, 19, 20], experimental determination of the nature of partial order in real materials is crucial.

Materials in which magnetic ions occupy a pyrochlore lattice of corner-sharing tetrahedra provide opportunities for realizing exotic frustrated states [21]. The frustrated pyrochlore antiferromagnet $\text{Gd}_2\text{Ti}_2\text{O}_7$ is a canonical partially-ordered system in which magnetic Gd^{3+} ions ($S = 7/2$) undergo two phase transitions at $T_1 = 1.1$ K and $T_2 = 0.75$ K [22–26]. Both low-temperature (LT; $T \ll T_2$) and intermediate ($T_2 < T < T_1$) phases have magnetic propagation vector $\mathbf{k} = (\frac{1}{2} \frac{1}{2} \frac{1}{2})$ [27, 28] and are partially ordered, as shown by the coexistence of magnetic Bragg and diffuse scattering in polarized-neutron scattering measurements [28]. However, the LT magnetic structure of $\text{Gd}_2\text{Ti}_2\text{O}_7$ has not yet been conclusively solved, for two reasons. First, the large neutron absorption cross-section of natural Gd makes neutron-scattering experiments on large crystals challenging. Second, most experimental probes are

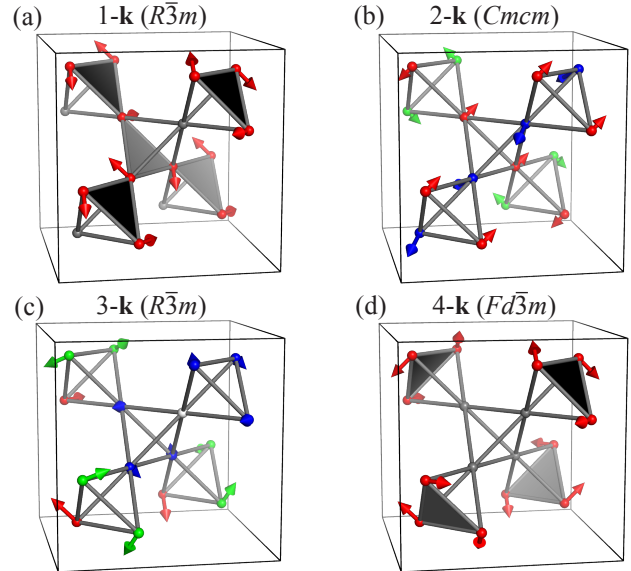


FIG. 1. Basic candidate structures for $\text{Gd}_2\text{Ti}_2\text{O}_7$, showing (a) 1- \mathbf{k} , (b) 2- \mathbf{k} , (c) 3- \mathbf{k} , and (d) 4- \mathbf{k} structures. The symmetry of each structure is labeled. A single crystallographic unit cell is shown in each case; spin orientations are reversed in adjacent unit cells because of the $\mathbf{k} = (\frac{1}{2} \frac{1}{2} \frac{1}{2})$ propagation vector. Spin directions are shown as arrows with lengths proportional to the ordered moment magnitude μ_{ord} . Arrows of different colors indicate symmetry-inequivalent magnetic sites, and paramagnetic sites with zero μ_{ord} in (a) and (d) are shown as grey spheres.

unable to distinguish a magnetic structure that orders with a single $\mathbf{k} = (\frac{1}{2} \frac{1}{2} \frac{1}{2})$ wavevector (“1- \mathbf{k} structure”) from structures that superpose symmetry-equivalent $\mathbf{k} \in \langle \frac{1}{2} \frac{1}{2} \frac{1}{2} \rangle$ (n - \mathbf{k} struc-

tures, where $n \in \{2, 3, 4\}$ in this case). Four such candidate structures for $\text{Gd}_2\text{Ti}_2\text{O}_7$ are shown in Fig. 1. All are partially ordered, but each has a different modulation of the ordered magnetic moment μ_{ord} : the 1- \mathbf{k} and 4- \mathbf{k} structures have 25% interstitial paramagnetic sites, whereas 2- \mathbf{k} and 3- \mathbf{k} have more complicated μ_{ord} modulations. It was proposed in Ref. 28 that magnetic diffuse-scattering measurements support a 4- \mathbf{k} structure with cubic magnetic symmetry. However, this result was called into question by the observation of transverse magnetization in small applied magnetic fields $\mathbf{H} \parallel \langle 112 \rangle$ and $\langle 100 \rangle$, which is inconsistent with cubic symmetry [29, 30]. Moreover, theoretical modeling suggests that, while the intermediate structure is 4- \mathbf{k} and stabilized by fluctuations, the LT ground state may actually be 2- \mathbf{k} [9]—a striking prediction that has awaited a conclusive experimental test.

In this Letter, we experimentally determine the nature of partial magnetic order in $\text{Gd}_2\text{Ti}_2\text{O}_7$ using neutron-scattering measurements of isotopically-enriched powder and single-crystal samples, combined with symmetry analysis and spin-wave calculations. We show that the LT state of $\text{Gd}_2\text{Ti}_2\text{O}_7$ is actually 2- \mathbf{k} , in agreement with theory [9] but in contradiction with the interpretation of previous experiments [28]. Our paper is structured as follows. We first present single-crystal neutron-diffraction measurements in applied magnetic field that indicate non-cubic magnetic symmetry. We then perform a comprehensive symmetry analysis of candidate magnetic structures. Finally, we show that only a 2- \mathbf{k} structure is consistent with LT inelastic neutron-scattering (INS) data.

Measurements of magnetic Bragg intensities in zero applied magnetic field do not directly distinguish the structures shown in Fig. 1, due to spherical averaging in powder samples and averaging over degenerate magnetic domains in single crystals—a phenomenon known as the “multi- \mathbf{k} problem” [31]. To address this problem, we performed neutron-diffraction measurements on a $\sim 10 \text{ mm}^3$ single crystal using the WISH diffractometer at ISIS [32], and applied a weak magnetic field $\mathbf{H} \parallel [1\bar{1}0]$ to break the domain degeneracy at $T = 0.07 \text{ K}$ after zero-field cooling. The sample was cut from a larger crystal prepared by the floating-zone image furnace method [33, 34] and was 99.4% enriched with ^{160}Gd to minimize absorption. Domains of the cubic 4- \mathbf{k} structure are related only by translational and time-reversal symmetries and hence appear identical to neutrons, whereas domains of other n - \mathbf{k} structures have different diffraction patterns. A field-induced domain imbalance is therefore expected to leave the diffraction pattern unchanged *only* if the LT structure is 4- \mathbf{k} .

The magnetic field dependence of selected magnetic Bragg intensities is shown in Fig. 2. Magnetic Bragg peaks in the (hhl) plane disappear in small applied field $0.2 \leq \mu_0 H \leq 0.5 \text{ T}$, while the intensity of magnetic Bragg peaks outside the (hhl) plane increases. These observations are incompatible with the cubic 4- \mathbf{k} structure, unless the applied field actually caused a magnetic phase transition rather than a domain imbalance. This scenario occurs in $\text{Er}_2\text{Ti}_2\text{O}_7$ [35], but is unlikely in $\text{Gd}_2\text{Ti}_2\text{O}_7$, in which there is no experimental evidence for such a phase transition in either specific heat [25] or torque

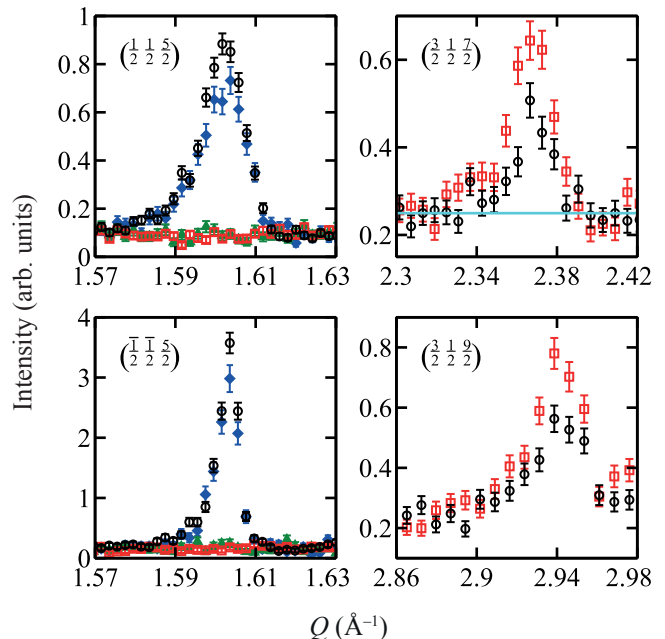


FIG. 2. Intensities of selected single-crystal magnetic Bragg peaks at different values of applied magnetic field $\mathbf{H} \parallel [1\bar{1}0]$ at $T = 0.07 \text{ K}$. Magnetic Bragg peaks are labelled in each panel; left-hand panels show peaks within the (hhl) plane and right-hand panels show peaks outside the (hhl) plane. Points are colored as follows: $\mu_0\mathbf{H} = 0$ (black hollow circles), $\mu_0\mathbf{H} = 0.1 \text{ T}$ (blue filled diamonds), $\mu_0\mathbf{H} = 0.2 \text{ T}$ (green filled triangles), and $\mu_0\mathbf{H} = 0.5 \text{ T}$ (red hollow squares). For clarity, only $\mu_0\mathbf{H} = 0$ and $\mu_0\mathbf{H} = 0.5 \text{ T}$ are shown in the right-hand panels. For the $(\frac{3}{2} \frac{1}{2} \frac{1}{2})$ peak, the integrated intensity is 0.11(2) units for $H = 0$ and 0.22(2) units for $\mu_0\mathbf{H} = 0.5 \text{ T}$, consistent with the expected doubling (the estimated background is shown as a light blue line).

magnetometry [29] measurements for $\mathbf{H} \parallel \langle 110 \rangle$ of less than 2 T at base temperature. The field-induced uniform magnetization is also too small to suppress magnetic Bragg peaks fully for $0.2 \leq \mu_0 H \leq 0.5 \text{ T}$ ($M \approx 0.2 \mu_B$ for $\mu_0 H \approx 0.2 \text{ T}$ [26, 30]). These observations strongly disfavor the cubic 4- \mathbf{k} structure, but do not distinguish candidate non-cubic structures.

To constrain further the LT magnetic structure, we reinterpret published powder-neutron diffraction data [28] using a comprehensive symmetry analysis. Fig. 3 shows data collected in the LT phase (0.25 K) using the D20 diffractometer at the ILL [36]. Nearly all the features of the data can be modeled using a single magnetic irreducible representation (“irrep”), denoted L_{1+} in Miller and Love’s notation [Fig. 3(a)] [37]. The L_{1+} model is the best currently available for $\text{Gd}_2\text{Ti}_2\text{O}_7$, and generates the four basic n - \mathbf{k} structures shown in Fig. 1. Crucially, however, the $(\frac{1}{2} \frac{1}{2} \frac{1}{2})$ magnetic Bragg peak observed in the 0.25 K experimental data is absent for the L_{1+} model [inset to Fig. 3(a)]. This result suggests that, while the L_{1+} irrep is the main contributor to the LT magnetic structure, at least one other irrep must also be present. We therefore tested the four possible combinations of L_{1+} with

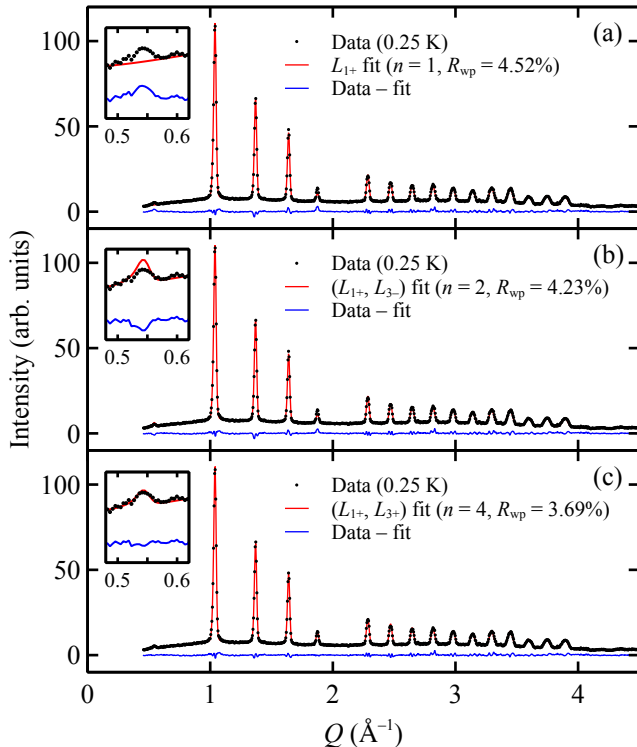


FIG. 3. Experimental powder neutron-diffraction data (from Ref. 28, $\lambda = 2.42 \text{ \AA}$) in the LT phase (0.25 K) and Rietveld fits for (a) the L_{1+} irrep, (b) the (L_{1+}, L_{3-}) irrep pair, and (c) the (L_{1+}, L_{3+}) irrep pair. Experimental data are shown as black points, fits as red lines, and data-fit as blue lines. For each model, the number of free parameters (magnetic distortion modes) n and the goodness-of-fit metric R_{wp} are shown. The insets show the $(\frac{1}{2}, \frac{1}{2}, \frac{1}{2})$ magnetic Bragg peak on an expanded scale.

one other irrep (L_{2+}, L_{3+}, L_{1-} , or L_{3-}). Only the (L_{1+}, L_{3-}) and (L_{1+}, L_{3+}) combinations allow nonzero intensity of the $(\frac{1}{2}, \frac{1}{2}, \frac{1}{2})$ peak and so are candidates. For each of these irrep pairs, we generated structural models using the Isodistort program [38, 39], and treated the magnetic distortion-mode amplitudes as free parameters which we optimized against our diffraction data using Topas Academic [40].

Fig. 3 compares fits to diffraction data for the single-irrep L_{1+} model with the two-irrep (L_{1+}, L_{3-}) and (L_{1+}, L_{3+}) models. The two-irrep models yield an improved overall fit to the data—in particular, to the $(\frac{1}{2}, \frac{1}{2}, \frac{1}{2})$ peak—by increasing the number of free parameters as indicated in Fig. 3. Unfortunately, the inclusion of an additional irrep also increases the number of candidate structures from four to 32 (see SM), all consistent with powder-diffraction data. We therefore apply the criterion that no site should have $\mu_{\text{ord}} > 7.0 \mu_{\text{B}}$ —the maximum value for $S = 7/2$ Gd^{3+} ions—which reduces the number of candidate structures to eight. Four of these are monoclinic (L_{1+}, L_{3-}) variants of the 1- \mathbf{k} structure, in which paramagnetic spins order with a small μ_{ord} [28]. However, these structures are disfavored by symmetry because the L_{3-} irrep

is not a symmetry-allowed secondary order parameter (SOP) here [38, 39]. The other four comprise three 2- \mathbf{k} structures and one 4- \mathbf{k} structure, of which only two (L_{1+}, L_{3+}) 2- \mathbf{k} structures contain a symmetry-allowed SOP. These two-irrep structures are consistent with the moment-length constraint, but the single-irrep 2- \mathbf{k} structure is not, and was therefore neglected in previous work [28]. Importantly, however, the moment-length constraint rules out all 3- \mathbf{k} structures, so we do not consider these further.

Since magnetic Bragg scattering does not fully distinguish candidate structures, we turn to high-resolution INS experiments. Measurements were performed using the DCS spectrometer at NIST [41] on a ~ 0.2 g portion of the powder sample studied in Ref. 28. An incident wavelength of 8 \AA yielded an energy resolution ≈ 0.025 meV (FWHM). Figs. 4(a) and 4(b) show background-subtracted powder INS data in the intermediate phase (0.77 K) and the LT phase (~ 0.05 K), respectively. The magnetic scattering at 0.77 K is broad in Q and E . By contrast, the LT data show two relatively flat modes at energies of approximately 0.06 meV and 0.17 meV. We performed additional INS measurements on a thin piece of our single crystal using the CNCS spectrometer at ORNL, which show that the background-subtracted single-crystal scattering integrated over $(h, k, l) = (0 \pm 1, 0 \pm 1, \frac{3}{2} \pm \frac{1}{2})$ resembles the powder data [Fig. 4(c)]. Our observation of a mode at very low energy (0.06 meV) is consistent with observations of low-energy dynamics in neutron spin echo [42] and muon-spin rotation [43, 44] experiments.

We use linear spin-wave theory to test models against the LT excitation spectrum. The minimal spin Hamiltonian for $\text{Gd}_2\text{Ti}_2\text{O}_7$ is given by

$$H = J_1 \sum_{\langle i,j \rangle} \mathbf{S}_i \cdot \mathbf{S}_j + J_2 \sum_{\langle\langle i,j \rangle\rangle} \mathbf{S}_i \cdot \mathbf{S}_j + D \sum_i (S_i^z)^2 + H_{\text{dip}}, \quad (1)$$

where J_1 and J_2 denote Heisenberg exchange interactions between nearest neighbor and next-nearest neighbor spin pairs, which are denoted by angle brackets $\langle \rangle$ and $\langle\langle \rangle\rangle$, respectively; D is a single-ion anisotropy term that arises from mixture of the excited ${}^6S_{7/2}$ atomic state into the ${}^8S_{7/2}$ ground state [45]; and H_{dip} is the long-ranged magnetic dipolar interaction with energy scale $D_{\text{dip}} S(S+1) = 0.84$ K [22]. We take $J_1 S(S+1) = 4.8$ K [22], and include a small ferromagnetic $J_2 = -0.04 J_1$ to stabilize $\mathbf{k} = (\frac{1}{2}, \frac{1}{2}, \frac{1}{2})$ ordering [9, 20, 22]. Electron-spin resonance (ESR) experiments find an easy-plane anisotropy that favors spin alignment perpendicular to local $\langle 111 \rangle$ axes [45]; we take $DS^2 = 1.5$ K to match our INS data. Further evidence for this Hamiltonian comes from measurements of the paramagnetic ($T > T_1$) diffuse scattering using the D4 diffractometer at the ILL [46], which are consistent with Monte Carlo simulations [47] for these parameters (see SM).

A prerequisite for spin-wave modeling is that the magnetic structure is a local energy minimum of Eq. (1). Using the SpinW program [48], we tested which of the eight candidate structures are proximate to energy minima by iteratively aligning each spin with its mean field and checking for sta-

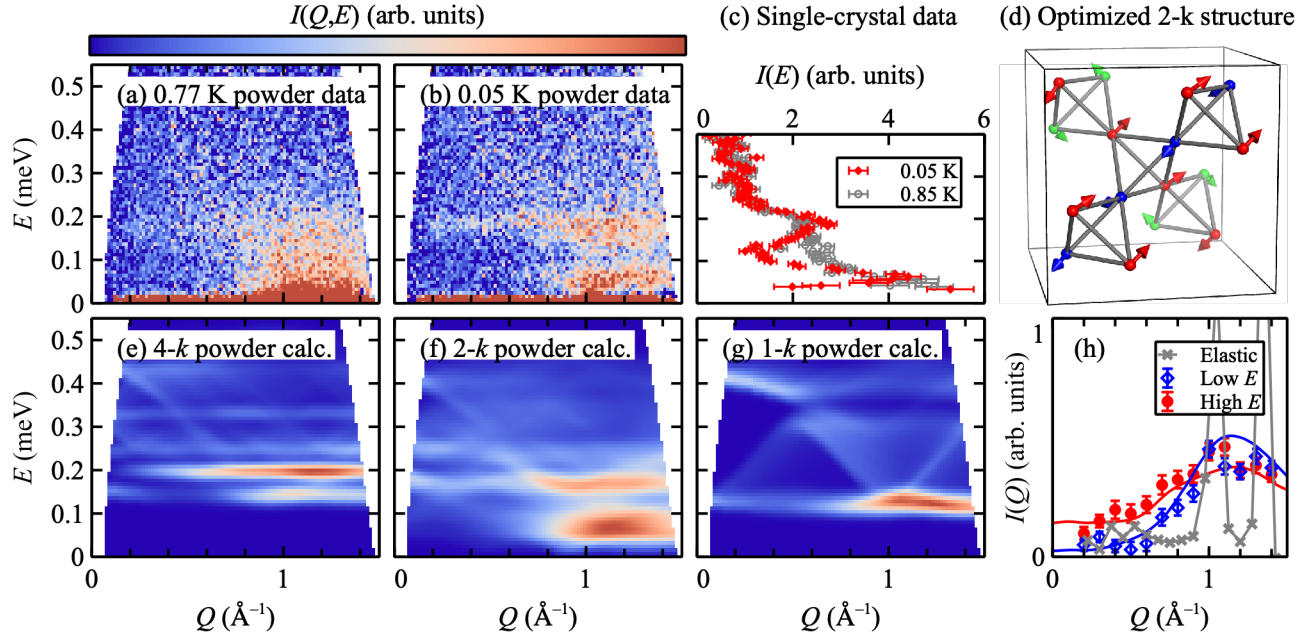


FIG. 4. (a) Inelastic neutron scattering data collected on a powder sample in the intermediate phase (0.77 K). (b) Powder INS data collected in the LT phase (~ 0.05 K). (c) Single-crystal INS data integrated over $(h, k, l) = (0 \pm 1, 0 \pm 1, \frac{3}{2} \pm \frac{1}{2})$ in the LT phase (0.05 K, solid red diamonds) and intermediate phase (0.85 K, empty grey circles). (d) Optimized 2- \mathbf{k} magnetic structure. (e) Powder-averaged linear spin-wave theory (LSWT) calculation for the L_{1+} 4- \mathbf{k} structure. (f) Powder LSWT calculation for the optimized (L_{1+}, L_{3+}) 2- \mathbf{k} structure discussed in the text. (g) Powder LSWT calculation for the L_{1+} 1- \mathbf{k} structure. (h) Powder INS data and spin-wave calculations at 0.05 K. Grey crosses show the measured elastic line ($-0.03 < E < 0.03$ meV; vertically shifted for clarity), empty blue diamonds show the measured low- E mode ($0.03 \leq E < 0.12$ meV), and filled red circles show the measured high- E mode ($0.12 \leq E \leq 0.21$ meV). Spin-wave calculations for low- E and high- E modes are shown as blue and red lines, respectively, and have been vertically scaled by the same factor to match the experimental data.

bility *via* the absence of imaginary spin-wave modes. Two candidate structures—one 2- \mathbf{k} and one 4- \mathbf{k} —are locally stable; both derive from the (L_{1+}, L_{3+}) irrep pair that yields the best fit to diffraction data [Fig. 3(c)]. By contrast, all candidate 1- \mathbf{k} structures with nonzero interstitial μ_{ord} are unstable. Fig. 4(d) shows the optimized (L_{1+}, L_{3+}) 2- \mathbf{k} structure, which resembles the refined structure (see SM). Compared to the L_{1+} 2- \mathbf{k} structure shown in Fig. 1(b), it has canted magnetic moments with more uniform magnitudes, $\mu_{\text{ord}}/\mu_{\text{B}} \in \{6.1(1), 4.6(1), 6.2(1)\}$ in a 1:1:2 ratio. However, the suppression of μ_{ord} compared to its theoretical value of $7.0\mu_{\text{B}}$ indicates partial ordering. Figs. 4(e), 4(f), and 4(g) show the calculated spin-wave spectra for the L_{1+} 4- \mathbf{k} , (L_{1+}, L_{3+}) 2- \mathbf{k} , and L_{1+} 1- \mathbf{k} structures, respectively. The 1- \mathbf{k} and 4- \mathbf{k} calculations strongly disagree with the 0.05 K experimental data. By contrast, the 2- \mathbf{k} calculation reproduces well the experimental data, most importantly the prominent low-energy (~ 0.06 meV) mode. The Q dependences of the low- E ($0.03 \leq E < 0.12$ meV) and high- E ($0.12 \leq E \leq 0.21$ meV) modes confirm this agreement [Fig. 4(h)]. We therefore conclude that the (L_{1+}, L_{3+}) 2- \mathbf{k} structure is the correct LT model.

Our experimental result that the LT structure of $\text{Gd}_2\text{Ti}_2\text{O}_7$ is 2- \mathbf{k} confirms state-of-the-art theoretical predictions [9] and solves a longstanding problem in the field of frustrated pyrochlore oxides. However, it contradicts a previous experi-

mental study [28], which proposed a 4- \mathbf{k} LT structure based on analysis of LT magnetic diffuse scattering. This study did not consider 2- \mathbf{k} structures, because the single-irrep 2- \mathbf{k} structure is unphysical and two-irrep 2- \mathbf{k} structures were not identified. It also assumed that ordered sites contribute no diffuse scattering; however, this assumption is incorrect because spin-wave scattering from ordered sites contributes to the energy-integrated diffuse intensity. In a fully-ordered system, $\mu_{\text{ord}}/\mu_{\text{B}} = 2S$, so that spin-wave scattering comprises $1/(S+1) = 22\%$ of the total intensity for $S = 7/2$. By contrast, partially-ordered $\text{Gd}_2\text{Ti}_2\text{O}_7$ has $\mu_{\text{ord}}/\mu_{\text{B}} < 2S$; by combining the refined values of μ_{ord} with the total-moment sum rule, we estimate that LT diffuse scattering comprises 46(2)% of the total intensity. Since the elastic scattering ($|E| < 0.03$ meV) is essentially flat away from Bragg peaks, whereas the inelastic scattering shows clear Q dependence [Fig. 4(h)], the LT diffuse scattering arises primarily from spin-wave fluctuations and not from static spin disorder or relaxational (paramagnetic) spin dynamics. The LT partial ordering of $\text{Gd}_2\text{Ti}_2\text{O}_7$ is therefore 2- \mathbf{k} with reduced ordered moments and enhanced spin-wave fluctuations. The orthorhombic symmetry of this structure is expected to drive a crystallographic distortion *via* spin-lattice coupling; however, our additional high-resolution powder neutron diffraction measurements do not show clear evidence of peak splitting, and

while a statistically-significant rhombohedral distortion could be refined (see SM), orthorhombic refinements were inconclusive due to their increased number of parameters. The intermediate-temperature partial ordering is also unusual. A 4-**k** structure is predicted to be stabilized by thermal fluctuations at T_1 [9], consistent with the absence of the $(\frac{1}{2} \frac{1}{2} \frac{1}{2})$ magnetic Bragg peak in the intermediate phase [28]. However, our 0.77 K INS data show only broad inelastic features, inconsistent with spin-wave predictions. This unexpected result may be explained if periodically-arranged paramagnetic sites in a 4-**k** structure suppress propagating spin-wave excitations, similar to the effect of paramagnetic impurities [49]. This intriguing possibility requires further theoretical investigation.

We are grateful to A. T. Boothroyd, S. T. Bramwell, M. J. Cliffe, M. J. P. Gingras, P. McClarty, M. Mourigal, P. J. Saines, and A. S. Wills for useful discussions, to O. Kirichek and the ISIS Sample Environment Group for cryogenic support, and to J. Makepeace and M. S. Senn for assistance with TOPAS 5. J.A.M.P.'s work at ORNL was supported by the Laboratory Directed Research and Development Program of Oak Ridge National Laboratory, managed by UT-Battelle, LLC for the US Department of Energy (manuscript preparation). J.A.M.P.'s work at Cambridge (magnetic structure analysis) was supported by Churchill College, University of Cambridge. J.A.M.P., A.B.C., and A.L.G. acknowledge financial support from the STFC, EPSRC (EP/G004528/2) and ERC (Ref: 279705). A portion of this research used resources at the Spallation Neutron Source, a DOE Office of Science User Facility operated by the Oak Ridge National Laboratory. Work at NHMFL (H.D.Z.) was supported by the NSF-DMR-1157490 and the State of Florida and U.S. Department of Energy. Experiments at the ISIS Neutron and Muon Source were supported by a beam time allocation from the STFC (U.K.).

* paddisonja@ornl.gov

† ross.stewart@stfc.ac.uk

- [1] R. Moessner, A. P. Ramirez, *Physics Today* **59**, 24 (2006).
- [2] R. Movshovich, M. Jaime, S. Mentink, A. A. Menovsky, J. A. Mydosh, *Phys. Rev. Lett.* **83**, 2065 (1999).
- [3] J. E. Greedan, C. R. Wiebe, A. S. Wills, J. R. Stewart, *Phys. Rev. B* **65**, 184424 (2002).
- [4] X. G. Zheng, *et al.*, *Phys. Rev. Lett.* **95**, 057201 (2005).
- [5] K. C. Rule, *et al.*, *Phys. Rev. B* **76**, 212405 (2007).
- [6] G. Cao, V. Durairaj, S. Chikara, S. Parkin, P. Schlottmann, *Phys. Rev. B* **75**, 134402 (2007).
- [7] G. Ehlers, C. Ritter, J. R. Stewart, A. D. Hillier, H. Maletta, *Phys. Rev. B* **75**, 024420 (2007).
- [8] T. J. Hayes, *et al.*, *Phys. Rev. B* **84**, 174435 (2011).
- [9] B. Javanparast, Z. Hao, M. Enjalran, M. J. P. Gingras, *Phys. Rev. Lett.* **114**, 130601 (2015).
- [10] M. E. Brooks-Bartlett, S. T. Banks, L. D. C. Jaubert, A. Harman-Clarke, P. C. W. Holdsworth, *Phys. Rev. X* **4**, 011007 (2014).
- [11] J. A. M. Paddison, *et al.*, *Nature Commun.* **7**, 13842 (2016).
- [12] S. Petit, *et al.*, *Nat. Phys.* **12**, 746 (2016).
- [13] C. Pfleiderer, *et al.*, *Nature* **427**, 227 (2004).
- [14] M. J. Rice, S. Strässler, G. A. Toombs, *Phys. Rev. Lett.* **32**, 596 (1974).
- [15] D. A. Keen, S. Hull, W. Hayes, N. J. G. Gardner, *Phys. Rev. Lett.* **77**, 4914 (1996).
- [16] M. T. Weller, O. J. Weber, P. F. Henry, A. M. Di Pumpo, T. C. Hansen, *Chem. Commun.* **51**, 4180 (2015).
- [17] C. Eames, *et al.*, *Nat. Commun.* **6** (2015).
- [18] E. Gregoryanz, *et al.*, *Science* **320**, 1054 (2008).
- [19] G.-W. Chern, R. Moessner, O. Tchernyshyov, *Phys. Rev. B* **78**, 144418 (2008).
- [20] A. S. Wills, *et al.*, *J. Phys.: Condens. Matter* **18**, L37 (2006).
- [21] J. S. Gardner, M. J. P. Gingras, J. E. Greedan, *Rev. Mod. Phys.* **82**, 53 (2010).
- [22] N. P. Raju, M. Dion, M. J. P. Gingras, T. E. Mason, J. E. Greedan, *Phys. Rev. B* **59**, 14489 (1999).
- [23] A. P. Ramirez, *et al.*, *Phys. Rev. Lett.* **89**, 067202 (2002).
- [24] P. Bonville, *et al.*, *J. Phys.: Condens. Matter* **15**, 7777 (2003).
- [25] O. A. Petrenko, M. R. Lees, G. Balakrishnan, D. M. Paul, *Phys. Rev. B* **70**, 012402 (2004).
- [26] O. A. Petrenko, M. R. Lees, G. Balakrishnan, *J. Phys.: Condens. Matter* **23**, 164218 (2011).
- [27] J. D. M. Champion, *et al.*, *Phys. Rev. B* **64**, 140407 (2001).
- [28] J. R. Stewart, G. Ehlers, A. S. Wills, S. T. Bramwell, J. S. Gardner, *J. Phys.: Condens. Matter* **16**, L321 (2004).
- [29] V. N. Glazkov, *et al.*, *J. Phys.: Condens. Matter* **19**, 145271 (2007).
- [30] O. A. Petrenko, M. R. Lees, G. Balakrishnan, V. N. Glazkov, S. S. Sosin, *Phys. Rev. B* **85**, 180412 (2012).
- [31] J. Kouvel, J. Kasper, *J. Phys. Chem. Solids* **24**, 529 (1963).
- [32] L. C. Chapon, *et al.*, *Neutron News* **22**, 22 (2011).
- [33] G. Balakrishnan, O. A. Petrenko, M. R. Lees, D. M. Paul, *J. Phys.: Condens. Matter* **10**, L723 (1998).
- [34] J. Gardner, B. Gaulin, D. Paul, *J. Cryst. Growth* **191**, 740 (1998).
- [35] J. P. C. Ruff, *et al.*, *Phys. Rev. Lett.* **101**, 147205 (2008).
- [36] T. C. Hansen, P. F. Henry, H. E. Fischer, J. Torregrossa, P. Convert, *Meas. Sci. Technol.* **19**, 034001 (2008).
- [37] A. P. Cracknell, B. L. Davies, S. C. Miller, W. F. Love, *Kronecker Product Tables. General Introduction and Tables of Irreducible Representations of Space Groups*, vol. 1 (Plenum, 1979).
- [38] B. J. Campbell, H. T. Stokes, D. E. Tanner, D. M. Hatch, *J. Appl. Crystallogr.* **39**, 607 (2006).
- [39] H. T. Stokes, D. M. Hatch, B. J. Campbell, Isotropy software suite, iso.byu.edu.
- [40] A. A. Coelho, *Topas Academic: General Profile and Structure Analysis Software for Powder Diffraction Data, version 5* (2012).
- [41] J. R. D. Copley, J. C. Cook, *Chem. Phys.* **292**, 477 (2003).
- [42] G. Ehlers, *J. Phys.: Condens. Matter* **18**, R231 (2006).
- [43] A. Yaouanc, *et al.*, *Phys. Rev. Lett.* **95**, 047203 (2005).
- [44] S. R. Dunsiger, *et al.*, *Phys. Rev. B* **73**, 172418 (2006).
- [45] V. N. Glazkov, *et al.*, *Phys. Rev. B* **72**, 020409 (2005).
- [46] H. E. Fischer, *et al.*, *Appl. Phys. A* **74**, s160 (2002).
- [47] J. A. M. Paddison, *et al.*, *J. Phys.: Condens. Matter* **29**, 144001 (2017).
- [48] S. Toth, B. Lake, *J. Phys.: Condens. Matter* **27**, 166002 (2015).
- [49] W. Brenig, A. L. Chernyshev, *Phys. Rev. Lett.* **110**, 157203 (2013).